Organic Electronics 57 (2018) 14–20

Contents lists available at ScienceDirect

Organic Electronics

journal homepage: www.elsevier.com/locate/orgel

High-performance CSA-PANI based organic phototransistor by elastomer gratings

Shivani Sharma, Robin Khosla, Subhashis Das, Hitesh Shrimali**, Satinder K. Sharma*

School of Computing and Electrical Engineering, Indian Institute of Technology Mandi, H.P, 175005, India

A R T I C L E I N F O

Keywords:
Organic field effect transistor (OFET)
Elastomer grating
Polyaniline (PANI)
Photo-responsivity
External quantum efficiency (EQE)

A B S T R A C T

A new and exciting pattern transfer method is presented to enhance the photoconductivity of Ag/CSA-PANI/PMMA/ITO, organic field effect transistor (OFET) by employing soft-lithography based grating over the channel region. The light is diffracted by the 265 nm gratings to enhance the UV (365 nm) activity of the channel material. The electrical characteristics of the grating-based OFET exhibited p-channel properties with the saturated hole mobility and the threshold voltage of $\sim 9.5 \times 10^{-5}$ cm^2/V-s and ~ -1.72 V respectively. The photo-generated charge carriers strongly influence the drain current in comparison to the dark condition. The External Quantum Efficiency of $\sim 2.45 \times 10^5$ establishes the photo-multiplication as a dominant factor for enhancement of the drain current. Moreover, the fabricated grating based OFET exhibited high photo-sensitivity and photo-responsivity of $\sim 1.16 \times 10^2$ and $\sim 7.33 \times 10^4$ A/W, respectively. Thus, the proposed soft-lithography grating based Ag/CSA-PANI/PMMA/ITO, OFET is an exceptional candidate for phototransistor applications.

1. Introduction

Organic semiconductors have captivated the recent research interest in the development of thin film transistors owing to the flexibility, cost-effective manufacturing and straightforward bulk scale fabrication techniques [1–3]. The Organic Field Effect Transistors (OFET) have an extensive range of applications such as gas sensing, smart cards, complementary logic, active matrix displays and photodetection [4], [5]. The OFET's sensitive to light are often termed as phototransistors which are used in numerous applications such as artificial eye detection, optical sensors [6], optical memory [7], and optical switches [8]. In literature, the phototransistor based on polymers such as naphthalene bisbenzimidazole [9], BPE-PTCDI [10], Pentacene [11], P3HT:PCBM [12], PDPP-DBTE [13], and conjugated polymer/fullerene blends [14] have been reported. In addition to these organic semiconductors, Polyaniline (PANI) is a potential p-type semiconductor material with higher stability, high electrical conductivity and low processing cost [15], [16]. Thus, it has been extensively explored for OFET [17–20], supercapacitors [21], [22], sensors [23], [24], medical applications [25] and optoelectronic applications [5], [26], [27].

In recent times, grating in the channel material has attracted the immense attention of optoelectronic community as it enhances the path length of photons. Thus, generates a higher number of electron-hole pairs which enhances the photoactivity of channel material [5]. Conventionally, the gratings in the channel are usually fabricated by expensive optical lithography and chemical etching techniques [28]. Conversely, Soft lithography [28–31] is a cost-effective non-photolithographic approach used to replicate microstructures by pouring the active elastomeric material on the surface of master mold. The significant increment of light trapping in the active semiconductor film for a specific wavelength depends on the geometric parameters of the diffraction grating [32]. Grating-induced light trapping and subsequent carrier enhancement have been extensively investigated by several groups such as Niggemann *et al.* [32], Seok-In Na *et al.* [33] for solar cells. Roman *et al.* demonstrated the effect of grating on the enhancement of EQE factor [34]. Campbell *et al.* [35] observed that textured surface entraps light in the semiconductor. Hsuet *et al.* [36] studied dual grating and its limitation in light trapping. Sasaki *et al.* and Havinga *et al.* [37], [38] reported that CSA doped polyaniline enhances the conductivity of the overall polymer on UV exposure. However, to the best of the author's knowledge, no report is available of using grating-based CSA doped polyaniline for phototransistor applications.

In this work, for the first time grating-based Ag/CSA-PANI/PMMA/ITO, OFET structure is fabricated by using spin coating and soft-lithography techniques. The electrical characteristics i.e. Output characteristics (I_{ds}-V_{ds}) and transfer characteristics (I_{ds}-V_{gs}) are measured in dark and under UV illumination with a 365 nm light (intensity ~ 300 μW/cm^2). The performance parameters of the phototransistor such as drain

* Corresponding author.
** Corresponding author.
E-mail addresses: hitesh@iitmandi.ac.in (H. Shrimali), satinder@iitmandi.ac.in (S.K. Sharma).

https://doi.org/10.1016/j.orgel.2018.02.031
Received 13 November 2017; Received in revised form 3 February 2018; Accepted 21 February 2018
Available online 23 February 2018

current, responsivity (R), photosensitivity and external quantum efficiency (EQE) are successfully analyzed in both accumulation and depletion mode. Further, the capacitive-voltage (C-V) characteristics of Ag/CSA-PANI/PMMA/ITO, structure are investigated to reveal the interface trapping properties. Furthermore, the surface morphology of deposited thin films and gratings are investigated by atomic force microscopy. Finally, the high performance of Ag/CSA-PANI/PMMA/ITO, OFET structure is supported by proposed model and energy band diagram.

2. Experimental

2.1. Materials and instruments

Fisher Scientific made monomer aniline (purity 99%), Oxidant Ammonium peroxydisulphate (APS) (purity 98%), and hydrochloric acid (HCl) is utilized to polymerize the aniline. Camphor sulfonic acid (CSA) was procured from Alfa Aesar and used as the doping material, whereas Merck made m-cresol (purity 99.5%) was the solvent. Elastomer cast for the Grating was prepared using commercially available Sylgard-184, PDMS kit, from Dow Corning (USA). The ITO coated glass (Sigma Aldrich) with the resistivity in the range of 8–12 Ω/cm^2 was used as a substrate. The PMMA (Poly (methyl methacrylate)) 950 A1 is obtained from Microchem. Note that, all the chemicals were utilized as received without any further purification.

The surface morphology of as-deposited CSA-polyaniline, the grating pattern and the PMMA dielectric were examined by using atomic force microscopy (AFM); Dimension Icon from Bruker) in tapping mode with a scan rate of ~0.5 Hz at room temperature. The high aspect ratio TESPA-HAR, AFM probe with resonant frequency 320–369 kHz and spring constant (k) of 20–80 N/m was used for AFM measurements. The thickness of the films was confirmed using Stylus Profilometer. The output (I_{ds}-V_{ds}) and the transfer characteristics (I_{ds}-V_{gs}) of the fabricated photo FET were measured using Keithley SCS 4200 characterization system under dark and light illumination using UV lamp (365 nm) of power 300 μW/cm^2.

2.2. Synthesis of polyaniline

PANI is synthesized chemically by the oxidation process at ~0–5 °C. Initially, 0.2 M aniline monomer is dissolved in 100 ml of HCl (1 M), and the solution cooled at 0 °C. Then, 33 ml of 0.8 M solution of ammonium peroxydisulphate ($(NH_4)_2S_2O_8$) in HCl (1 M) solution was added dropwise to the monomer aniline solution; continuous stirring changes the color to green which physically signifies polymerization. The stirring was continued for next 4 h at ~0 °C to achieve the desired molecular weight of the polymer. Next, the solution was kept overnight at 0 °C to allow settling down of the resultant polymerized PANI precipitates, followed by acetone and then DI water rinse to remove the aniline oligomers. Further, the precipitates were vacuum dried at 60 °C for 12 h to obtain emeraldine PANI powder. Ensuing to this, the CSA powder is added to Polyaniline powder to enhance the conductivity followed by addition of an m-cresol solvent in the ratio of PANI (1): CSA (0.5): m-cresol (10). Finally, the solution is stirred at 90 °C for 2 h followed by ultrasonic treatment for 15 min to obtain a homogeneous CSA-PANI solution.

2.3. Fabrication of organic field effect transistor (OFET)

OFET is fabricated with top contact/bottom gate geometry to minimize the contact resistance. Fig. 1 shows the process steps followed for fabrication of phototransistor. Initially, indium tin oxide (ITO) coated glass is cleaned with soapy solution followed by DI water rinse then sonicated in Acetone, ethanol and DI water for 15 min each (Fig. 1(a)). To form the insulator/dielectric layer, PMMA 950 A1 was spin-coated on the ITO coated glass at 1000 rpm for 60 s, and the curing

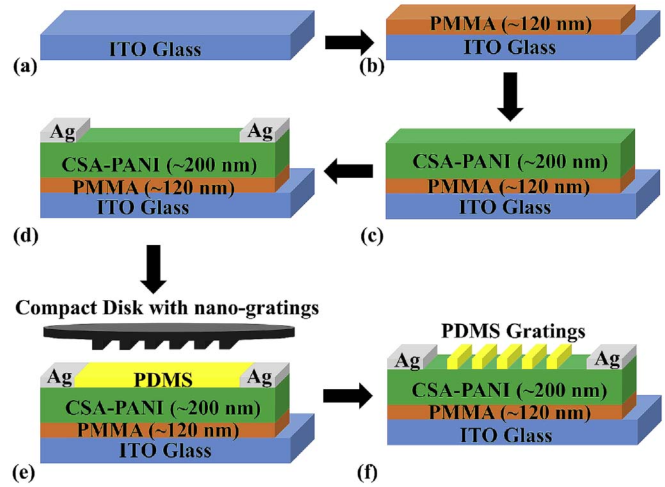

Fig. 1. Process flow used for fabrication of Nano-Grating Polyaniline based Field Effect Transistor.

process was carried out at 60 °C for 20 min (Fig. 1(b)). The process was repeated four times to achieve a thickness of ~120 nm. The semiconductor layer was formed using CSA doped polyaniline film by spin coating at 3000 rpm for 90 s and cured at 65 °C for 30 min (Fig. 1(c)) and thickness obtained after 15 cycles were ~200 nm. For metal electrodes, Ag (99.99% purity) ~100 nm thin films were deposited by thermal evaporation at an ultimate pressure of $\sim 2 \times 10^{-6}$ torr using shadow mask with the channel length (L) of 100 μm and channel width (W) of ~1 mm (Fig. 1(d)).

The PDMS elastomer was prepared from Sylgard-184 by the addition of part B crosslinking agent to part A in the ratio of 1:10 to get desired flexibility. This elastomer solution was manually stirred for 10 min, and then ultrasonication was done for 5 min in a water bath. The desiccating process in vacuum was carried out to remove the air bubbles. Thereafter, the PDMS mold was spin-coated at 3000 rpm for 60 s to obtain ~110 nm thick film over the channel region (Fig. 1(e)). The optical storage disk was used as the master mold to transfer pattern on the PDMS coated channel region. A force of 7.85 N was applied while desiccating the sample for 1 h to efficiently transfer pattern on the channel region. Thereafter, the soft curing process was carried out at 35 °C for 4 h to ensure the cross-linking of PDMS chains and further to prevent the deformation of the PDMS surface structure (negative DVD pattern) a hard curing was obtained by subjecting a thermal treatment for 2 h at 90 °C. This results in the grating formation as shown in Fig. 1(f).

3. Results and discussions

Fig. 2 (a) illustrates the output characteristics of the bottom gated Ag/CSA-PANI/PMMA/ITO, OFET without gratings in dark condition. In a typical p-channel operating mode, a negative gate bias induced the accumulation of hole carriers at the interface between active semiconductor (CSA-PANI) and dielectric layer (PMMA). A linear increase in the drain current with the increase in drain voltage and a considerable saturation of the drain current after an increase in the applied drain voltage establishes the transistor action [39]. The output characteristics of the bottom gated Ag/CSA-PANI/PMMA/ITO, OFET with gratings in dark condition is shown in Fig. 2(b). On comparing the I_{ds} value of Ag/CSA-PANI/PMMA/ITO, OFET devices without and with gratings, it is observed that there is insignificant variation in I_{ds} value (~-3 to ~-13 nA with deviation in V_{gs} from +2 V to -2 V at V_{ds} of -4 V) which may be due to the isolation of the devices from environment due to elastomer gratings and hence increases the reliability of OFET. Further, Fig. 2 (c) and 2 (d) shows the output characteristics of the bottom gated Ag/CSA-PANI/PMMA/ITO, OFET without and with gratings under

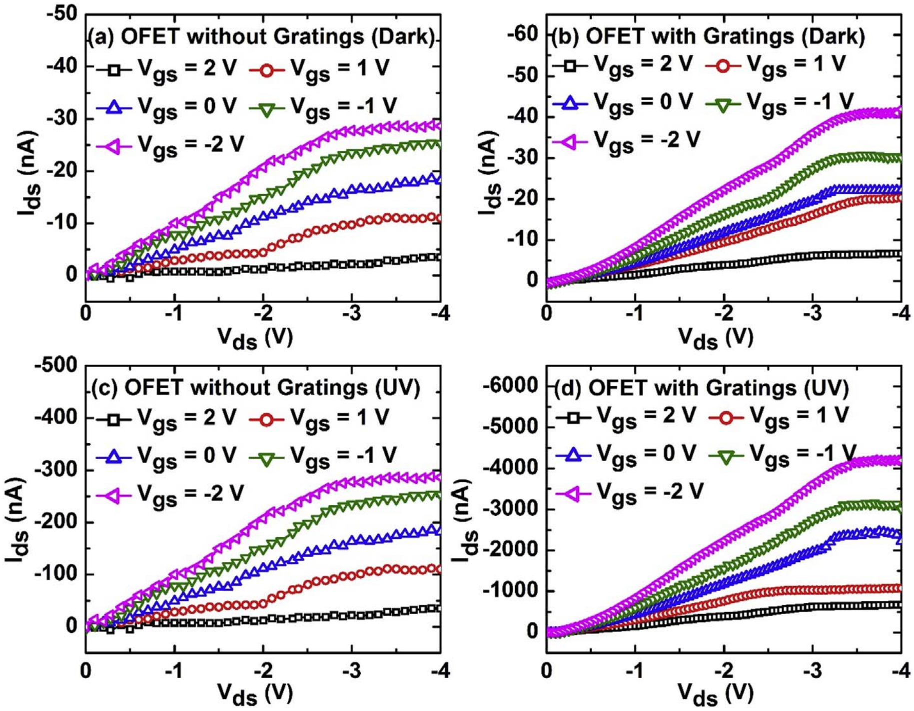

Fig. 2. Output characteristics (I_{ds}-V_{ds}) of Ag/CSA-PANI/PMMA/ITO Organic Field Effect Transistor (OFET) with variation in gate-source voltage. (a) OFET without Gratings and (b) OFET with Gratings under dark. (c) OFET without Gratings and (d) OFET with gratings under 365 nm UV illumination.

365 nm UV illumination, respectively. It is observed that the I_{ds} value (at V_{ds} of -4 V and V_{gs} of -2 V) increases from $\sim -2.8625 \times 10^{-8}$ A (Dark) to $\sim -2.8647 \times 10^{-7}$ (UV) in Ag/CSA-PANI/PMMA/ITO, OFET without grating, i.e., ~900% increase in I_{ds} value on UV illumination. On the Other hand, the I_{ds} value (at V_{ds} of -4 V and V_{gs} of -2 V) upsurges from $\sim -4.1924 \times 10^{-8}$ A (Dark) to $\sim -4.1952 \times 10^{-6}$ A (UV) in Ag/CSA-PANI/PMMA/ITO, OFET with gratings, i.e., ~9900% increase in I_{ds} value on UV illumination. Therefore, the large increase in the current with gratings under UV illumination is possibly due to the enhanced scattering/trapping of light by the gratings. Here, the contribution of photo-generated carriers may be due to (i) Exciton formation and subsequent dissociation into free carriers by an electric field; or (ii) Photo-injection of carriers from the metal source/drain electrodes into the polyaniline [40].

When the p-type device operates in the saturation region, the standard equation is modulated to:

$$I_{ds\,sat} = \mu C_i \frac{W}{L}(V_{gs} - V_{th})^2, \; V_{ds} > (V_{gs} - V_{th}) \tag{1}$$

where μ, C_i, W, L, V_{gs}, V_{th}, V_{ds} are hole mobility, capacitance of dielectric layer, channel width, channel length, gate voltage, threshold voltage and drain voltage, respectively. When it operates in the linear region, it is modulated as:

$$I_{ds\_lin} = \mu C_i \frac{W}{L}\left[\{V_{gs} - V_{th}\}V_{ds} - \frac{1}{2}V_{ds}^2\right], \; V_{ds} < (V_{gs} - V_{th}) \tag{2}$$

Fig. 3 shows the transfer characteristics ($I_{ds}^{1/2}$-V_{gs}) of the OFET in the dark and with light illumination for the V_{ds} bias of -2 V. The hole mobility and the threshold voltage are calculated using the following relation:

$$I_{ds\,sat}^{1/2} = \mu C_i \left(\frac{W}{L}\right)^{\frac{1}{2}} (V_{gs} - V_{th}) \tag{3}$$

From Fig. 3 (a), the hole mobility and the threshold voltage in the dark were calculated as $\sim 9.55 \times 10^{-5}$ cm^2/V-s and ~ -1.72 V, respectively. Whereas the same parameters in the illumination were computed as $\sim 7.3 \times 10^{-3}$ cm^2/V-s and ~ -1.58 V, respectively from

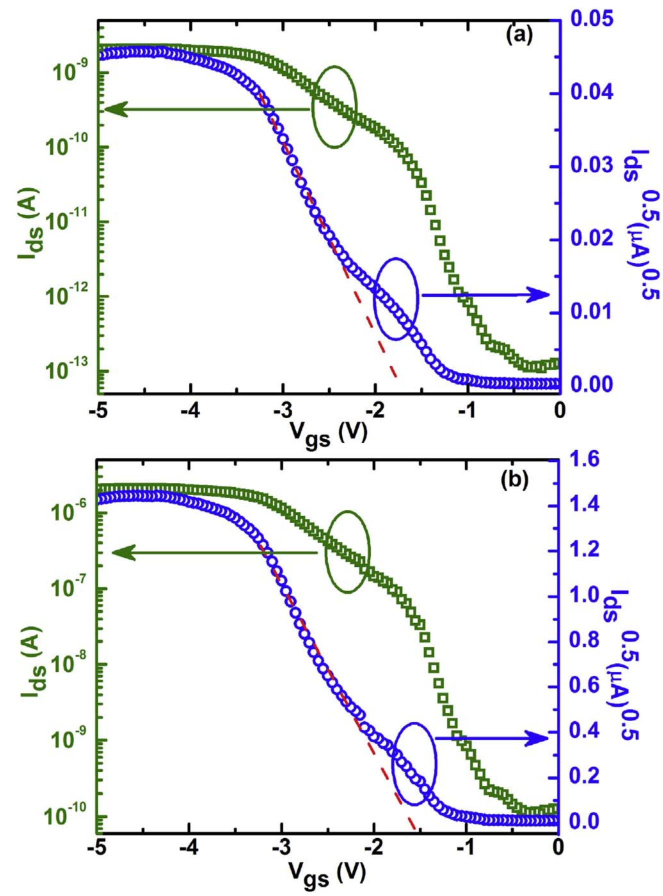

Fig. 3. Transfer characteristics (I_{ds}-V_{gs}) along with $I_{ds}^{1/2}$-V_{gs} of the device (a) in dark (b) in illumination of 365 nm wavelength at $V_{ds} = -2$ V.

Fig. 3 (b). The reduced value of V_{th} in the case of UV illumination substantiates the increase in carrier concentration in the channel region. The effect of UV irradiation has also been delineated in terms of the change in transconductance of the device using the following equation [39]:

$$g_m = 2\frac{I_{ds}}{V_{gs} - V_{th}} \tag{4}$$

The extracted values of g_m at the off state under dark condition are ~4.7 nA/V and ~25.4 nA/V for the linear and saturation regime, respectively. Upon UV illumination, the g_m has been increased to 0.53 μA/V and 3.6 μA/V for linear and saturation regime, respectively, affirming the enhanced performance of the fabricated devices.

Photosensitivity is an important parameter which dictates the performance of the device. It can be defined as the ratio of the photocurrent to the dark current (I_{ph}/I_{dark}) [5]. The photosensitivity of the device is calculated as $\sim 1.06 \times 10^2$ in linear region before $V_{ds} = -3$ V and $\sim 1.05 \times 10^2$ in the saturation region after $V_{ds} = -3$ V for $V_{gs} = 0$ V. The illumination of the light causes to increase the conductivity by increasing the generation of electron-hole pair, hence there is high photosensitivity at the turn off state. The other parameter which plays a prominent role in the phototransistor is the photo-responsivity, defined as the ratio of the photogenerated current (I_{ph}) to the optical power (P_{opt}) input to the device area, related as [5]:

$$R = \frac{I_{ph}}{P_{opt}} = \frac{I_{illum} - I_{dark}}{P_{inc}A} \tag{5}$$

where, P_{inc} is the power of the incident light per unit area. The responsivity of the device in the depletion mode and in accumulation mode are $\sim 1.35 \times 10^4$ A/W and $\sim 7.33 \times 10^4$ A/W, respectively, which is better than that of the previous reports summarized in Table 1 [40–42].

Furthermore, the external quantum efficiency (η) of the phototransistor is defined as the ratio of the photo-generated carrier that enhances the drain current to the number of photons incident on the channel, expressed as [10]:

$$\eta = \left(\frac{I_{illum} - I_{dark}}{P_{inc}\lambda_{peak}Ae}\right)hc \tag{6}$$

Where h, c, e, A and λ_{peak} are the Planck's constant, speed of light, unit charge, area of the channel exposed and wavelength of the incident light. The device exhibits very high η value of $\sim 4.51 \times 10^4$ and $\sim 2.45 \times 10^5$ in linear and saturation mode, respectively. The enhanced η value confirms the photo multiplication of charge carriers. The similar observations were made by Yu *et al.* [10], Huang *et al.* [43], and Li *et al.* [44]. Higher EQE value predicts the defect-free nature of the film, and it may be due to the scattering of the light which causes an increase in the intensity of light responsible for photo-generated current [38], [39].

In order to confirm, the quality of the Ag/CSA-PANI/PMMA/ITO, MOS structure used in the present work, the C-V characteristics are obtained by shorting the drain and source to form one electrode as shown in Fig. 4. Here, the cyclic C-V characteristics are obtained by sweeping the gate voltage from positive (+3 V) to negative (−3 V) to positive (+3 V). Initially, when the gate voltage is negative, the channel is in accumulation mode and majority charge carriers (holes) are accumulated close to the PMMA/CSA-PANI interface. As the gate voltage approaches towards positive direction, the majority charge carriers holes starts to depleted and finally ends up with strong inversion at low and high frequency as shown in Fig. 4. It indicate that in depletion region there is no conduction path near the PMMA/CSA-PANI interface [49].

Table 1
Progress of the phototransistors.

Semiconductor Channel Material	Photo-sensitivity	Photo-Responsivity	EQE	Reference
Naphthalene bis-benzimidazole	93.4	14.3 mAW^{-1}	–	[42]
poly(3-hexylthiophene)	3800	250 AW^{-1}	–	[40]
Hydrazonic Squaraine	–	340 AW^{-1}	74000	[46]
Graphene sensitized by Cu2-xSe Nanocrystals	–	2400 AW^{-1}	–	[47]
Copper Phthalocyanine	–	430 AW^{-1}	–	[48]
CSA-PANI	106	73,300 AW^{-1}	245000	Present Work

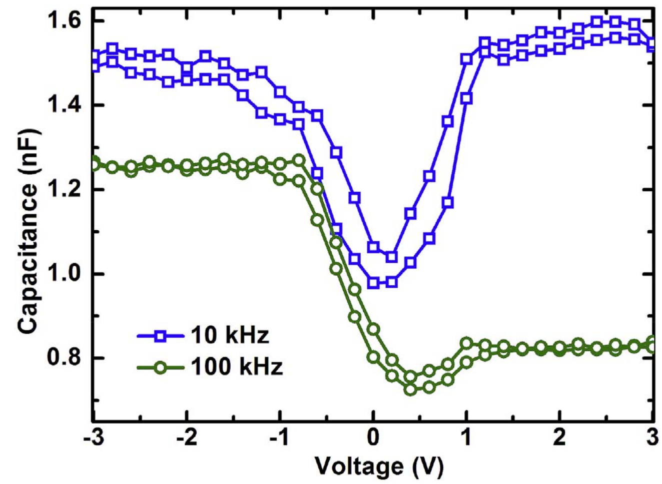

Fig. 4. Capacitance-Voltage characteristics of the MOS device formed by ITO/PMMA/CSA-PANI/Ag.

Thus, the C-V characteristics confirm the p-type nature of CSA-PANI. The maximum oxide capacitance at −3 V in accumulation is ~1.51 nF at 10 kHz, which decreases to ~1.26 nF at 100 kHz. This trivial variation in accumulation capacitance of ~0.25 nF with variation in frequency from 10 to 100 kHz may be due to more charge carries resonance at driving voltage at low frequency [50]. Since, the accumulation layer is formed if the input frequency is less than relaxation time [51]. Moreover, the cyclic C-V curves showed negligible hysteresis of ~0.3 V, which confirms the high-quality PMMA/CSA-PANI interface with low charge trapping desired for device applications [49], [52], [53].

Further, to confirm the topology of gratings and investigate the surface morphology of deposited thin films, surface analysis using AFM is desired. The surface morphology of the dielectric layer plays a crucial role in the charge transport near the junction and the interface of the semiconductor because only a few layers of the semiconductor near the dielectric layer take part in the accumulation of the charge [54]. The roughness of the dielectric layer may lead to the charge trapping at dielectric/semiconductor interface [45]. Smooth pattern transfer and uniform line/space distribution across the channel region has been clearly observed, as evident from Fig. 5(a) and (b). The grating size is estimated to be ~265 nm from AFM surface micrographs. In this work, we have fabricated the gratings based on the principle of the Bragg's grating law which states that grating period (i.e. distance between centres of adjacent gratings) should be larger than the wavelength which is intended for enhanced light trapping in the system. So, the grating size significantly effects the device performance, e.g. the selectivity for scattering of 365 nm. The basic Bragg's law for monochromatic waves incident normal to the gratings is expressed as follows [54]:

$$p = \frac{\lambda}{\sin(\theta)} \tag{7}$$

where p is the grating period, λ is the wavelength, and θ is the half angle between the two standing waves. Thus, using Bragg's law, to

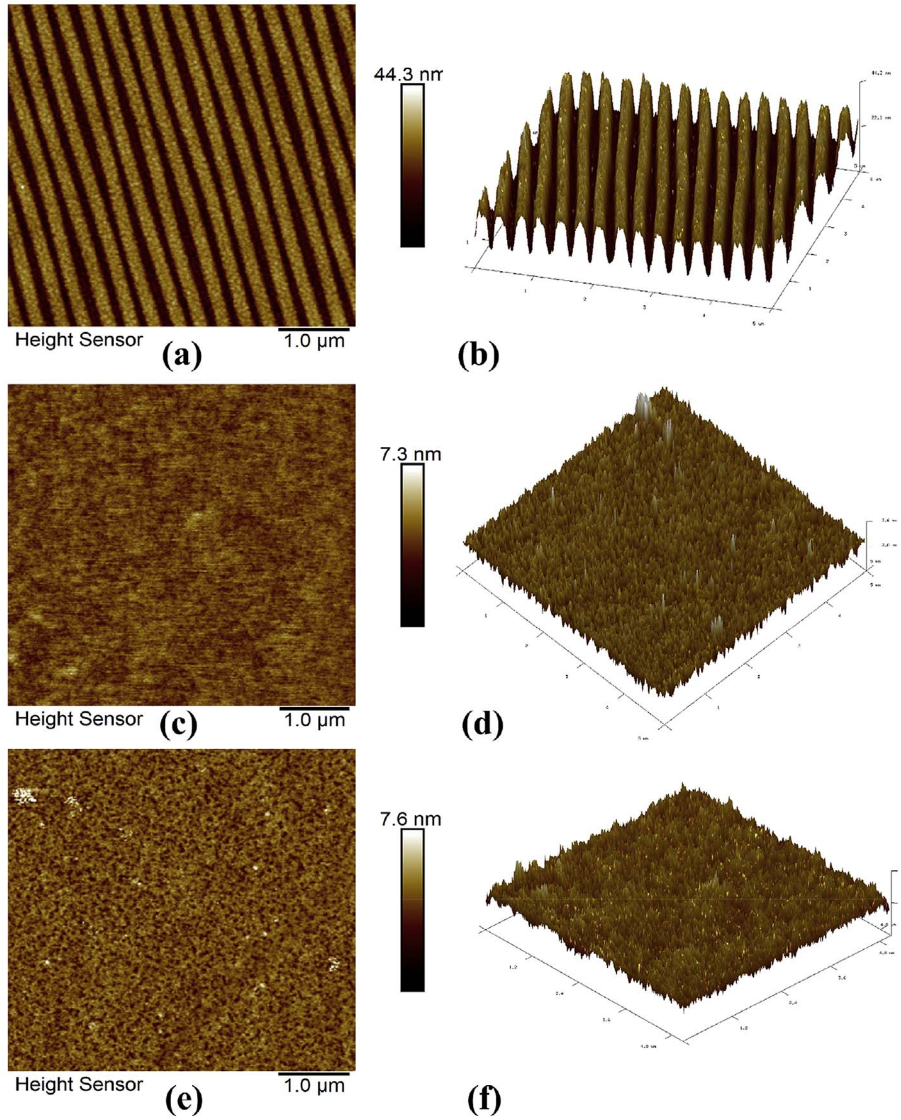

Fig. 5. AFM surface micrographs (2-D and 3-D) of nano gratings on CSA-PANI/PMMA/ITO structure ((a) and (b)), PMMA 950 A1 thin films on ITO ((c) and (d)), and CSA doped polyaniline thin films on PMMA/ITO structure.

detect 365 nm wavelength incident perpendicular to sample surface, i.e. half angle of 90°, the grating period is estimated to be ∼365 nm. Therefore, for selective scattering/trapping of 365 nm wavelength, the symmetric grating period must be equivalent to ∼365 nm [55]. Hence, in the proposed system, the grating period is taken to be ∼375 nm which is confirmed from AFM surface micrographs (Fig. 5 (a)) using image analysis software.

The height of the gratings plays a vital role in the phase of the light reflected by the grating which further influences the absorption of the light in the material. Catchpole *et al.* [56] stated that there will be maximum power absorption when the phase shift of the light with the grating is the odd multiple of 180°. The phase shift of the grating is related as:

$$\Delta\phi = \frac{2\pi d \Delta n}{\lambda} \tag{8}$$

where Δn is the difference between the refractive index of the grating material (∼1.4 for PDMS) and the surrounding (∼1 for air), λ is the wavelength of the incident light (∼365 nm), and d is the depth/height of the grating. Here, the height of the grating induced over the channel material has been calculated from the AFM surface micrographs (Fig. 5(b)) to be ∼45 nm. Therefore, using equation (8), the phase of the reflected light is calculated to be odd multiple of 180°, which is best required for the large light path length and hence high light absorption in the material [56]. It must be noted that, if the height of the grating is increased or decreased then the reflection/transmittance of the light becomes prominent instead of scattering/trapping in the material which will reduce the responsivity of the devices [57], [58], [59]. Therefore, the optimum value of grating height ∼45 nm is used for fabrication of the phototransistor by transferring the pattern on the PDMS elastomer.

Fig. 5(c) and (d) show 2-d and 3-d AFM surface micrographs of the solution processed PMMA A1 thin films. It has been noticed that the PMMA film formed is quite uniform with the rms roughness of ∼4.49 Å. Fig. 5(e) and (f) represent 2-d and 3-d surface morphology of the solution processed CSA-PANI thin film on the PMMA dielectric with the rms roughness of ∼6.19 Å.

The accumulation of holes under the dark conditions is achieved at the PMMA/CSA-PANI interface as shown in Fig. 6(a). Further, on UV illumination, the gratings fabricated over the semiconductor (PANI) channel region leads to the increased path length of the light which is responsible for more light diffraction/trapping in the semiconductor. The diffracted light increases the exposure area of UV irradiation in the semiconductor that finally leads to the increase in electron-hole pair

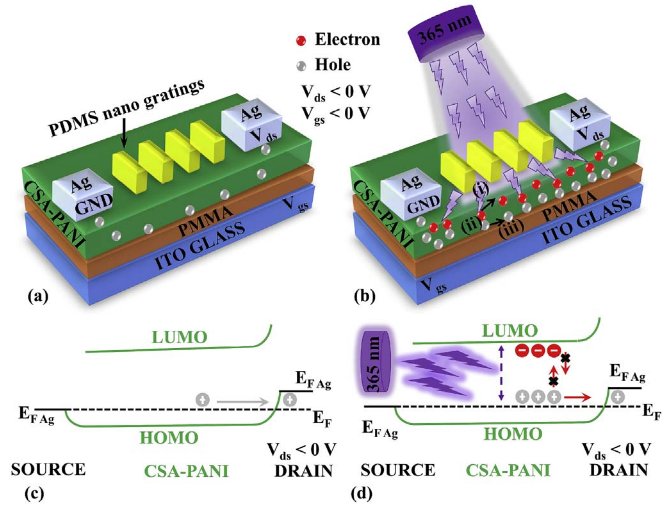

Fig. 6. Device structure and charge accumulation under (a) Dark, (b) 365 nm UV illumination. Energy band diagram of the organic FET in off-state under (c) Dark and (d) 365 nm UV illumination.

generations (Fig. 6(b) inset (ii)). Consequently, the drain current of the device increases signifying the enhanced photogenerated charge carrier, as depicted in Fig. 6(b). It might be due to that the applied drain voltage drags the photo-generated holes away from their recombination centres (Fig. 6(b) inset (iii)) and similarly more elucidated by the proposed band model as shown in Fig. 6(c) and (d). The charge recombination centres within the semiconductor are confined due to the upward band bending of the CSA-PANI caused by the negative drain bias. Eventually, the increased hole collection for the same applied drain voltage leads to the decrease in the threshold voltage.

4. Conclusion

In Summary, gratings over the channel material have been successfully realized to enhance the photo-activity of the CSA doped polyaniline organic semiconductor channel material. A new soft lithography based method of pattern transfer has been introduced. The gratings over the semiconductor channel showed excellent light diffraction behaviour resulting in the significant increase in drain current under UV illumination and substantial high photo-responsivity $\sim 7.33 \times 10^4$ A/W. The low surface roughness of the PMMA film facilitates the device performance by reducing the interface roughness. The increased path length of the photons due to the diffraction induced by the grating in the channel material produces the photo multiplication effect which is confirmed by the EQE factor of the device.

Acknowledgment

The authors would like to acknowledge the research fellowship from MHRD, Govt. of India. Author S. Das thankfully acknowledges the financial support from Science and Engineering Research Board, Govt. of India under National Post-Doctoral Fellow scheme with file no. PDF/2016/003135. This work was financially supported by the seed grant project IIT/SG/SKS/27, Indian Institute of Technology (IIT), Mandi, (H.P), India.

References

[1] G. Blanchet, J. Rogers, Printing techniques for plastic electronics, J. Imag. Sci. Technol. 47 (4) (2003) 296–303.
[2] S.H. Ahn, L.J. Guo, High-speed roll-to-roll nanoimprint lithography on flexible plastic substrates, Adv. Mater. 20 (11) (2008) 2044–2049.
[3] F. Templier, B. Aventurier, P. Demars, J.L. Botrel, P. Martin, Fabrication of high performance low temperature poly-silicon backplanes on metal foil for flexible active-matrix organic light emission diode displays, Thin Solid Films 515 (19) (2007) 7428–7432 SPEC. ISS.
[4] G.H. Gelinck, et al., Flexible active-matrix displays and shift registers based on solution-processed organic transistors, Nat. Mater. 3 (2) (2004) 106–110.
[5] S. Sharma, R. Khosla, D. Deva, H. Shrimali, S.K. Sharma, Fluorine-chlorine co-doped TiO2/CSA doped polyaniline based high performance inorganic/organic hybrid heterostructure for UV photodetection applications, Sens. Actuat. A Phys. 261 (2017) 94–102.
[6] O.A. Ogawa M, Radiolabeled apoptosis imaging agents for early detection of response to therapy, Sci. World J. 2014 (2014).
[7] M. Gu, X. Li, Y. Cao, Optical storage arrays: a perspective for future big data storage, Light Sci. Appl. 3 (5) (2014) e177.
[8] H. Sirringhaus, 25th anniversary article: organic field-effect transistors: the path beyond amorphous silicon, Adv. Mater. 26 (9) (2014) 1319–1335.
[9] W. Boukhili, C. Tozlu, M. Mahdouani, S. Erten-Ela, R. Bourguiga, Illumination and dipole layer effects on the density of state distribution in n-type organic thin film phototransistors based on naphthalene bis-benzimidazole: experiment and modeling, Microelectron. Eng. 179 (2017) 37–47.
[10] H. Yu, Z. Bao, J.H. Oh, High-performance phototransistors based on single-crystalline n-channel organic nanowires and photogenerated charge-Carrier behaviors, Adv. Funct. Mater. 23 (5) (2013) 629–639.
[11] S. Okur, F. Yakuphanoglu, E. Stathatos, "High-mobility pentacene phototransistor with nanostructured SiO2 gate dielectric synthesized by sol-gel method, Microelectron. Eng. 87 (4) (2010) 635–640.
[12] M. Yasin, et al., P3HT: PCBM blend based photo organic field effect transistor, Microelectron. Eng. 130 (2014) 13–17.
[13] M. Kim, et al., Flexible organic phototransistors based on a combination of printing methods, Org. Electron. Phys. Mater. Appl. 15 (11) (2014) 2677–2684.
[14] N. Marjanović, et al., Photoresponse of organic field-effect transistors based on conjugated polymer/fullerene blends, Org. Electron. Phys. Mater. Appl. 7 (4) (2006) 188–194.
[15] H. Wang, J. Lin, Z.X. Shen, Polyaniline (PANi) based electrode materials for energy storage and conversion, J. Sci. Adv. Mater. Devices 1 (3) (2016) 225–255.
[16] M.A.E. Hafizah, A. Bimantoro, Andreas, Andreas, A. Manaf, Synthesized of conductive polyaniline by solution polymerization technique, Proced. Chem. 19 (2016) 162–165.
[17] S. Chao, M.S. Wrightor, Characterization of a 'Solid-State' polyaniline-based transistor: water vapor dependent characteristics of a device employing a poly(vinyi alcohol)/phosphoric acid solid-state electrolyte, J. Am. Chem. Soc. 109 (22) (1987) 6627–6631.
[18] J. Bhadra, D. Sarkar, Field effect transistor fabricated from polyaniline-polyvinyl alcohol nanocomposite, Indian J. Phys. 84 (6) (2010) 693–697.
[19] C.M. Hangarter, et al., Electronic transport characteristics of electrolyte-gated conducting polyaniline nanowire field-effect transistors, Synth. Met. 13 (1) (1997) 1308–1314.
[20] A.E.-S. Karim Amer, Shaker Ebrahim, Mohamed Feteha, Moataz Soliman, Organic Field Effect Transistor Based on Polyaniline - Dodecylbenzene Sulphonic Acid for Humidity Sensor, (2017), pp. 440–447.
[21] S. A. Ansari, N. Parveen, T. H. Han, M. O. Ansari, and M. H. Cho, "Fibrous polyaniline@manganese oxide nanocomposites as supercapacitor electrode materials and cathode catalysts for improved power production in microbial fuel cells," Phys. Chem. Chem. Phys., vol. 18, no. 13, pp. 9053–9060, 2016.
[22] Y. Gawli, et al., 3D polyaniline architecture by concurrent inorganic and organic acid doping for superior and robust high rate supercapacitor performance, Sci. Rep. 6 (1) (2016) 21002.
[23] A. Suea-Ngam, P. Rattanarat, K. Wongravee, O. Chailapakul, M. Srisa-Art, Droplet-based glucosamine sensor using gold nanoparticles and polyaniline-modified electrode, Talanta 158 (2016) 134–141.
[24] J. Liang, et al., Sensitive electrochemical determination of hydrogen peroxide using copper nanoparticles in a polyaniline film on a glassy carbon electrode, Anal. Lett. 2719 (2017) no. November, p. 00032719.2017.1343832.
[25] C. You, et al., Near-infrared light and pH dual-responsive targeted drug Carrier based on core-crosslinked polyaniline nanoparticles for intracellular delivery of cisplatin, Chem. Eur J. 23 (no. 22) (2017) 5352–5360.
[26] H. Wang, G. Yi, X. Zu, X. Jiang, Z. Zhang, H. Luo, A highly sensitive and self-powered ultraviolet photodetector composed of titanium dioxide nanorods and polyaniline nanowires, Mater. Lett. 138 (2015) 204–207.
[27] T. Barman, A.R. Pal, Plasmonic photosensitization of polyaniline prepared by a novel process for high-performance flexible photodetector, ACS Appl. Mater. Interfaces 7 (4) (2015) 2166–2170.
[28] P. Kumar, R. Khosla, M. Soni, D. Deva, S.K. Sharma, A highly sensitive, flexible SERS sensor for malachite green detection based on Ag decorated microstructured PDMS substrate fabricated from Taro leaf as template, Sens. Actuator. B Chem. 246 (2017) 477–486.
[29] M.G. Kim, H. Alrowais, S. Pavlidis, O. Brand, Size-scalable and high-density liquid-metal-based soft electronic passive components and circuits using soft lithography, Adv. Funct. Mater. 27 (3) (2017).
[30] F. Bella, A. Verna, C. Gerbaldi, Patterning dye-sensitized solar cell photoanodes through a polymeric approach: a perspective, Mater. Sci. Semicond. Process. (2017) 1–7 July.
[31] M.A. Unger, Monolithic microfabricated valves and pumps by multilayer soft lithography, Science (80-.) 288 (5463) (2000) 113–116.
[32] M. Niggemann, M. Glatthaar, A. Gombert, A. Hinsch, V. Wittwer, Diffraction gratings and buried nano-electrodes - architectures for organic solar cells, Thin Solid Films 451–452 (2004) 619–623.
[33] S.I. Na, et al., Surface relief gratings on poly(3-hexylthiophene) and fullerene blends for efficient organic solar cells, Appl. Phys. Lett. 91 (17) (2007) 1–4.

[34] L.S. Roman, et al., Trapping light in polymer photodiodes with soft embossed gratings, Adv. Mater. 12 (3) (2000) 189–195.
[35] P. Campbell, M.A. Green, Light trapping properties of pyramidally textured surfaces, J. Appl. Phys. 62 (1) (1987) 243–249.
[36] W.C. Hsu, et al., Mismatched front and back gratings for optimum light trapping in ultra-thin crystalline silicon solar cells, Opt. Commun. 377 (2016) 52–58.
[37] I. Sasaki, J. Janata, M. Josowicz, Stabilization of electronic properties of (1R)-(-)-10-camphorsulfonic acid doped polyaniline by UV irradiation, Polym. Degrad. Stab. 92 (7) (2007) 1408–1416.
[38] E.E. Havinga, M.M. Bouman, E.W. Meijer, A. Pomp, M.M.J. Simenon, Large induced optical activity in the conduction band of polyaniline doped with (1S)-(+)-10-camphorsulfonic acid, Synth. Met. 66 (1) (1994) 93–97.
[39] B. Razavi, Design of Analog CMOS Integrated Circuits. New York: McGraw-Hll Higher Education.
[40] T. Pal, M. Arif, S.I. Khondaker, High performance organic phototransistor based on regioregular poly(3-hexylthiophene), Nanotechnology 21 (32) (2010) 325201.
[41] W. Rekab, M.A. Stoeckel, M. El Gemayel, M. Gobbi, E. Orgiu, P. Samorì, High-performance phototransistors based on PDIF-CN2 solution-processed single fiber and multifiber assembly, ACS Appl. Mater. Interfaces 8 (15) (2016) 9829–9838.
[42] C. Tozlu, S. Erten-Ela, S. Icli, Photoresponsive n-channel organic field effect transistor based on naphthalene bis-benzimidazole with divinyltetramethyl disiloxane-bis (benzo-cyclobutene) gate insulator, Sens. Actuat. A Phys. 161 (1–2) (2010) 46–52.
[43] J. Huang, Y. Yang, Origin of photomultiplication in C 60 based devices, Appl. Phys. Lett. 91 (20) (2007) 1–4.
[44] L. Li, et al., Achieving EQE of 16,700% in P3HT: PC71BM based photodetectors by trap-assisted photomultiplication, Sci. Rep. 5 (2015) 9181.
[45] M. Irimia-Vladu, et al., Vacuum-processed polyaniline-C60 organic field effect transistors, Adv. Mater. 20 (20) (2008) 3887–3892.
[46] L. Caranzi, G. Pace, M. Sassi, L. Beverina, M. Caironi, Transparent and highly responsive phototransistors based on a solution-processed, nanometers-thick active layer, embedding a high-mobility electron-transporting polymer and a hole-trapping molecule, ACS Appl. Mater. Interfaces (2017) p. acsami.7b05259.
[47] J. Lee, et al., Graphene phototransistors sensitized by Cu2-xSe nanocrystals with short amine ligands, J. Phys. Chem. C 121 (9) (2017) 5436–5443.
[48] J.H. Jung, et al., High-performance UV–vis–NIR phototransistors based on single-crystalline organic semiconductor–gold hybrid nanomaterials, Adv. Funct. Mater. 27 (6) (2017).
[49] W. Brutting, Physics of Organic Semiconductors Handbook, WIEY-VCH Verlag GmbH&Co. KGaA, 2005.
[50] S. Scheinert, G. Paasch, S. Pohlmann, H.H. Horhold, R. Stockmann, Field effect in organic devices with solution-doped arylamino-poly-(phenylene-vinylene), Solid State Electron. 44 (5) (2000) 845–853.
[51] R. Khosla, S.K. Sharma, Frequency dispersion and dielectric relaxation in post-deposition annealed high-k erbium oxide metal–oxide–semiconductor capacitors, J. Vac. Sci. Technol. B 36 (1) (2018) 12201.
[52] R. Khosla, P. Kumar, S.K. Sharma, Charge trapping and decay mechanism in post deposition annealed Er 2 O 3 MOS capacitors by nanoscopic and macroscopic characterization, IEEE Trans. Device Mater. Reliab. 15 (4) (2015) 610–616.
[53] R. Khosla, E.G. Rolseth, P. Kumar, S.S. Vadakupudhupalayam, S.K. Sharma, J. Schulze, "Charge trapping analysis of metal/Al 2 O 3/SiO 2/Si, gate stack for emerging embedded memories, IEEE Trans. Device Mater. Reliab. 17 (1) (2017) 80–89.
[54] F. Dinelli, M. Murgia, P. Levy, M. Cavallini, F. Biscarini, D.M. De Leeuw, Spatially correlated charge transport in organic thin film transistors, Phys. Rev. Lett. 92 (11) (2004) 116802–1.
[55] D. K. Darin Madzharov, Rahul Dewan, Influence of front and back grating on light trapping in microcrystalline thin-film silicon solar cells S2/OPTICS EXPRESS A95, Sol. Energy Mater. Sol. Cells 74 (19) (2002) 457–467.
[56] Z. Yu, A. Raman, S. Fan, Limit of nanophotonic light-trapping in solar cells, Conf. Rec. IEEE Photovolt. Spec. Conf. 18 (2010) 76–78 no. September.
[57] K.R. Catchpole, M.A. Green, A conceptual model of light coupling by pillar diffraction gratings, J. Appl. Phys. 101 (6) (2007).
[58] J. Rao, S. Varlamov, Light trapping in thin film polycrystalline silicon solar cell using diffractive gratings, Energy Proced. 33 (2013) 129–136.
[59] D. Madzharov, et al., Influence of front and back grating on light trapping in microcrsystalline thin-film silicon solar cells S2/OPTICS EXPRESS A95, Opt. Soc. Am. 74 (19) (2002) 457–467.